XX IMEKO World Congress
Metrology for Green Growth
September 9–14, 2012, Busan, Republic of Korea

# IMAGE PROCESSING OF DATA OBTAINED IN EDDYCURRENT NON-DESTRUCTIVE EVALUATION OF METALLIC PLATES

*A. Lopes Ribeiro, H. Geirinhas Ramos, D. Pasadas, T. Rocha*

Instituto de Telecomunicações, Instituto Superior Técnico, Lisboa, Portugal, arturlr@ist.utl.pt

**Abstract:** This paper describes the usage of a planar excitation coil in a nondestructive testing experiment, using the eddy current method under sinusoidal excitation. After scanning a rectangular area on the metallic surface of the specimen under test, the probe signals obtained by a giant magneto-resistor sensor, were displayed in the form of a 2D representation. To determine the geometric form of the defects inside an aluminum plate, an inversion algorithm was tested. The algorithm is based on a kernel method. It uses the Discrete Fourier Transform (DFT) and Tikhonov regularization to obtain the spatial distribution of currents inside the aluminum plate.

**Keywords:** non-destructive evaluation; eddy-currents; ill-posed problems; Tikhonov regularization.

## 1. INTRODUCTION

The nondestructive evaluation of materials and parts is nowadays an activity in growing expansion, which has gathered the attention of industrial and academic communities. One method in use employs eddy currents to evaluate the integrity of metallic specimens [1]. This method uses an excitation coil to apply a primary time-varying magnetic field to the part under test. The electromotive forces developed inside the material give origin to the eddy currents which generate a secondary magnetic field of detectable amplitude. This field contains the information concerning the material non-homogeneities.

## 2. EXPERIMENTAL SETUP

Our system uses a planar excitation coil and sinusoidal excitation [2]. In the central region of the excitation coil the current tracks are parallel and evenly distributed in order to obtain, in the metallic plate to be tested, a primary magnetic field with uniform amplitude under that central region. Figure 1 depicts the current tracks on the planar excitation coil which was printed on a circuit board.

The secondary magnetic field generated by the eddies of current inside the metal is detected using a giant magneto-resistance sensor [3](GMR). The detectability of the GMR sensor is improved by inserting the sensing axis parallel to the excitation current lines. If the part under test is homogeneous with a plane boundary, the lines of current inside the material have the same orientation as the excitation current, and the resulting magnetic field will be perpendicular to the GMR sensing axis. Thus the GMR magnetometer will not sense any field in the case that the material is free of defects. If the metal under the GMR probe has defects, such as a crack, the eddy current lines deviate from their orientation and the secondary magnetic field components shall appear in the direction of the GMR sensing axis.

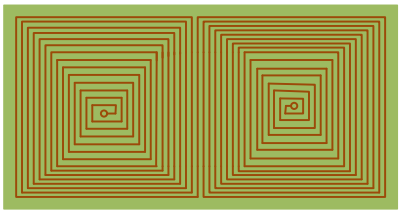

Figure 1. The planar excitation coil with current tracks parallel and equally spaced to produce a spatially uniform magnetic field in the central zone.

Figure 2 represents the experimental setup to scan a rectangular portion of an aluminum plate where some artificial cracks were included. The planar probe with the planar coil, a GMR sensor and an instrumentation amplifier with gain G=46 dB, were positioned over the plate by a xy-positioning system. The scan was performed by steps of 0.5 mm on both axes. The sinusoidal excitation current was delivered by a trans-admittance amplifier driven by a commercial Agilent function generator. The GMR output signal is acquired using a NI-USB-6251 acquisition board at the sampling frequency $f_S$= 1.2 MS/s. The complete system works under the control of a Labview program installed in a desktop personal computer.

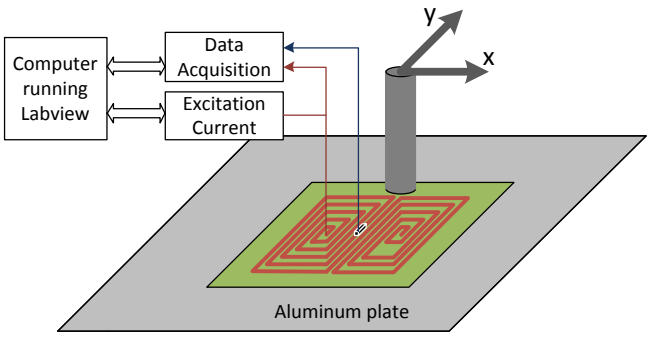


Figure 2. The planar excitation coil is moved over an aluminum plate and the GMR output signal is acquired.

The GMR sensor was polarized using a small permanent magnet to set the working point in the ascending linear branch of the v-shaped characteristic [4].

The Labview program controls the xy-position of the probe. The GMR output signal processing is performed by a 3-parameter sine-fitting algorithm [5] implemented in Labview as well. The excitation frequency is given and the algorithm determines the amplitude of the output GMR voltage, the DC-offset and the phase relative to the excitation current.

## 3. ACQUIRED DATA

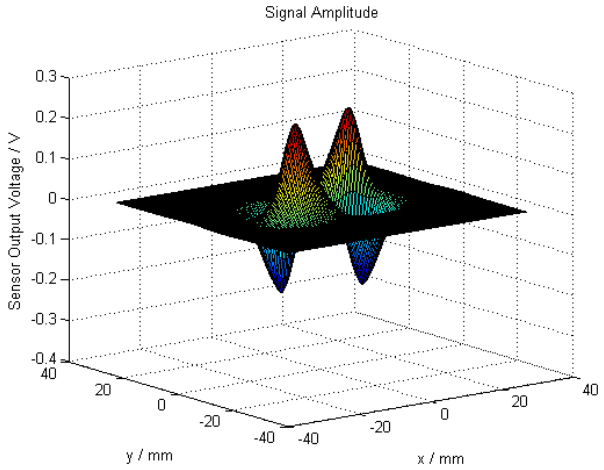


Figure 3. The GMR output voltage when the probe scans an aluminum plate with a straight crack.

The result presented in figure 3 was obtained with the probe oriented in such a way that the excitation currents in the immediate vicinity of the GMR sensor were oriented perpendicularly to the crack. Thus, the induction electric field is also perpendicular to the crack, but the eddy currents must deviate around it. This eddy current perturbation produces a magnetic field with component on the y-direction. If the plate were homogeneous the magnetic field produced by the eddy currents was confined to the x-direction and could not be sensed by the GMR. This situation happens on the regions near the boundary on Fig.3.

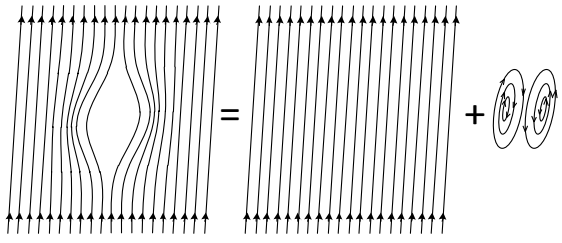


Figure 4. The disturbed lines of current are divided into parallel and divergence free lines.

As illustrated in Fig.4 the eddy currents on the plate may be divided in two parts. The first part is the current that is present when there are no flaws in the plate. This current has straight lines in the same direction of the excitation currents, but in opposition with them. When a flaw is present in the plate, e.g. a crack, the eddy currents are perturbed. This current perturbation is the second part into which the total eddy currents were divided. The perturbation currents exhibit zero divergence and may be considered as a summation of dipolar currents. Figure 4 represents the separation of the current inside the plate into the non-perturbed plus the perturbation eddies.

## 4. INVERSION ALGORITHM

The proposed inversion algorithm is based on the decomposition of the current perturbation in elemental current dipoles. As represented in Fig.5 each current dipole circulates on the square edges that constitute the elements of a virtual grid over the plate surface.

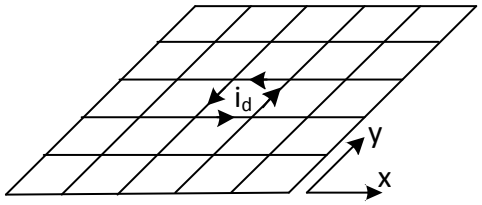


Figure 5. The plate surface is divided into squares with length equal to the pace of the positioning system. Dipole current $i_d$ circulates on the square edges.

The inversion problem consists on the determination of the circulating current on every elemental square of the grid. One important function to be determined is the field that would be sensed by the GMR if only one single square element (0.5×0.5 mm) in the grid contains a unitary current. This function was determined by considering that the unitary current flows on the edges of a rectangle, the distance between the metallic surface and the plane where the GMR moves is equal to d=1 mm, and noting that the GMR just senses the magnetic field component $H_y$. The calculation was performed using the Biot-Savart [6] law and the result is presented graphically in Fig. 6.

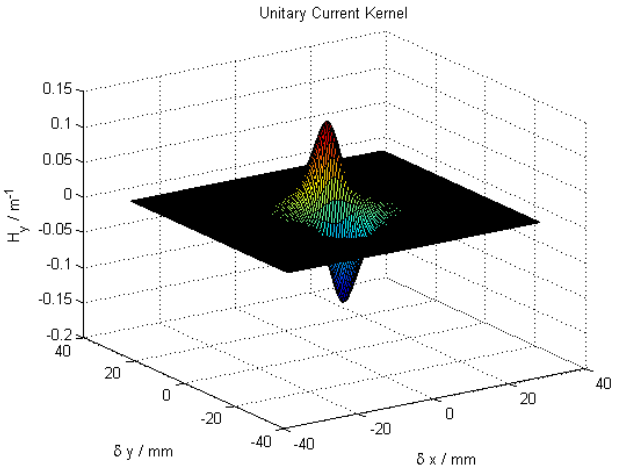


Figure 6. The field $h_y$ resulting from a unitary current in a single rectangular grid element.

The field $h_y$ may be considered the kernel of the transformation that maps the dipolar perturbation current density in the surface of the metallic plate into the actual measured data $H_y$ represented in Fig.3. The transformation is represented as the following convolution integral:

$$H_y(x,y) = \iint_{SA} h_y(x-x',y-y')I_d(x',y')dx'dy' \qquad (1)$$

The integral is extended to the scanned area *SA* and $I_d$ represents the distribution of the actual dipolar currents. The proposed inversion problem consists in the determination of $I_d$ from the data $H_y$ knowing the kernel $h_y$. The discretized form of (1) is:

$$H_y(m,n) = \sum_{k,l} h_y(m-k,n-l)I_d(k,l) \qquad (2)$$

being the square loops of current referred by the indexes (*k*,*l*) and the nodes where $H_y$ is computed referred by (*m*,*n*).

It is well known that the Fourier transform changes the convolution into a simple multiplication. Thus, it is recommended to use it here in the discrete form. By applying the DFT to (2) we obtain:

$$\hat{H}_y = \hat{h}_y \times \hat{I}_d \qquad (3)$$

In (3) the DFT is represented by the hat over the variables.

The temptation to obtain the DFT of $I_d$ by performing the direct division from (3) would lead to a loose end

$$\hat{I}_d = \frac{\hat{H}_y}{\hat{h}_y} . \qquad (4)$$

The impossibility to obtain the direct inversion from (4) is due to the presence of some noise in the data. The noise is especially harmful in the higher frequencies because the kernel in the denominator of (4) tends to zero at those frequencies, as it is shown in Fig.7.

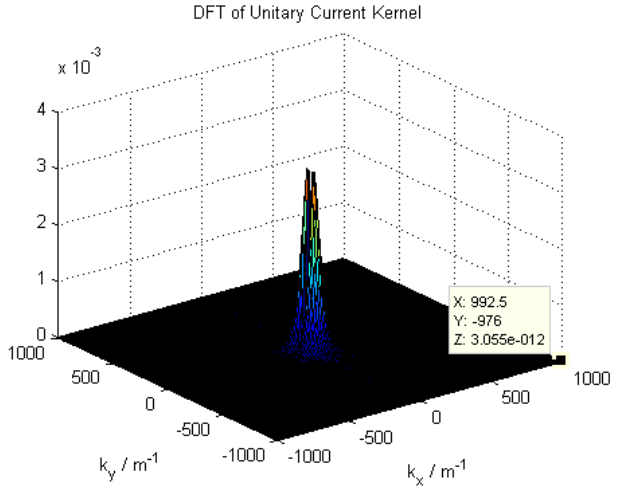


Figure 7. For the higher frequencies, the kernel $\hat{h}_y$ tends to zero.

The example depicted in Fig. 7 shows that, for the highest frequencies, the kernel DFT assumes values of the order of $10^{-12}$.

It is advisable, from now on, to separate the data into a noiseless component $\hat{H}_y^0$ and the noise $\hat{\eta}$:

$$\hat{H}_y = \hat{H}_y^0 + \hat{\eta} \qquad (5)$$

The dipolar current density is now expressed as the sum of a current distribution that would be obtained if the acquired data were noiseless with the term that includes the effect of noise.

$$\hat{I}_d = \frac{\hat{H}_y^0}{\hat{h}_y} + \frac{\hat{\eta}}{\hat{h}_y} = \hat{I}_d^0 + \frac{\hat{\eta}}{\hat{h}_y} \qquad (6)$$

We shall use Tikhonov regularization [7] to overcome the inversion difficulty. The kernel DFT is changed to

$$\hat{h}_y^\mu = \frac{|\hat{h}_y|^2 + \mu}{\hat{h}_y^*} \quad , \quad \hat{h}_y = \lim_{\mu \to 0} \hat{h}_y^\mu \qquad (7)$$

where $\mu > 0$ is the regularization parameter and * represents the complex conjugate. The choice of the optimum value of the regularization parameter was made, starting with large values of $\mu$ and checking smaller values until the resulting image begins to degrade. The inversion process may proceed by using the inverse DFT of the regularized dipolar current density:

$$\hat{I}_d^\mu = \frac{\hat{H}_y}{\hat{h}_y^\mu} \qquad (8)$$

Note that the relation (8) may be written in the form

$$\hat{I}_d^\mu = \frac{\hat{h}_y^*}{|\hat{h}_y|^2 + \mu}\hat{H}_y = \frac{|\hat{h}_y|^2}{|\hat{h}_y|^2 + \mu}\frac{\hat{H}_y}{\hat{h}_y} = \hat{W}_\mu \frac{\hat{H}_y}{\hat{h}_y} \qquad (9)$$

showing that the Tikhonov regularization is equivalent to a low-pass filter $\hat{W}_\mu$ actuating in the frequency domain.

## 5. RESULTS

The result obtained from (9) is converted to the direct space by using the Inverse Discrete Fourier Transform (IDFT).

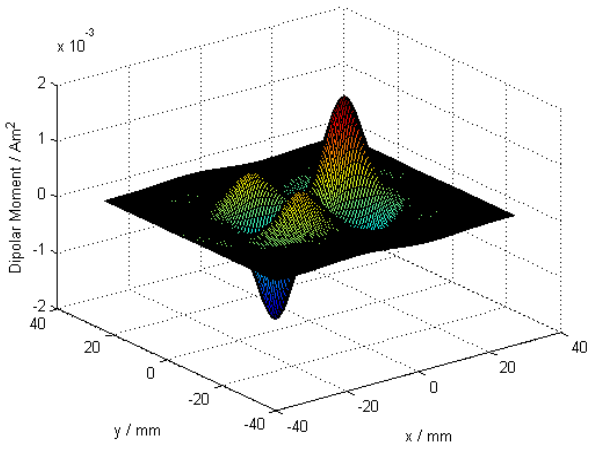


Figure 8. Dipolar current density in a crack zone.

The dipolar current density, as represented in Fig.8, is converted to the usual current density vector representation using the following transformation:

$$\begin{cases} J_x(m,n) = \left[ I_d(m+1,n) - I_d(m-1,n) \right] / 2 \\ J_y(m,n) = \left[ I_d(m,n-1) - I_d(m,n+1) \right] / 2 \end{cases} \quad (10)$$

With this transformation the current loops $I_d(m,n)$ are converted to the map of current density perturbation presented in Fig.9.

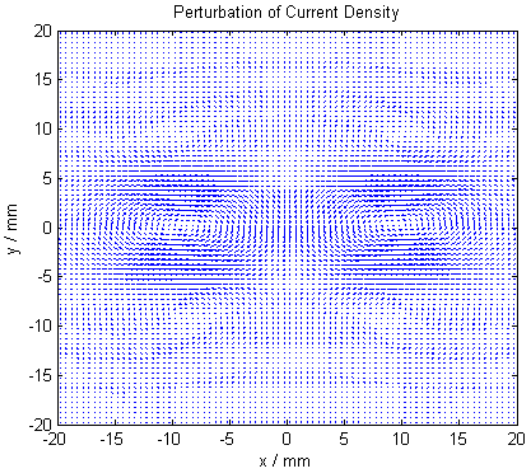


Figure 9. Eddies of perturbation currents.

Figure 9 shows the perturbation currents forming two eddies around the crack edges. In Fig.10 it is depicted a detail of the previous graphic showing how this virtual current circulates around the right edge.

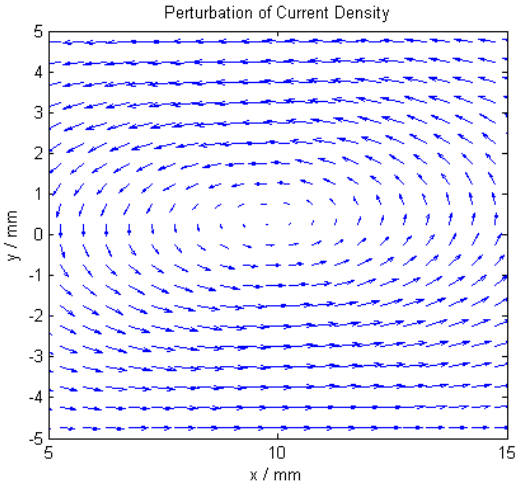


Figure 10. Detail of Fig.9.

It is now possible to reconstruct the real current density by adding a constant current density $J_y$ with amplitude equal to the amplitude of the perturbation current in the middle point between the two vortices and reversed signal. The final result is represented in Fig.11.

## 6. CONCLUSION AND DISCUSSION

In this paper we have used the Tikhonov regularization to obtain the distribution of the eddy currents around a crack in an aluminium plate subject to a non-destructive test using sinusoidal excitation.

The result presented in Fig.11 shows the current deviating from the crack. However, due to the low-pass filtering of the inversion scheme some residual current is seen to flow through the crack, which is located at (-10<x<10;y=0).

Nevertheless, the method is powerful enough to proceed with the research of more accurate regularization schemes.

It is important that the determination of the geometric form of the defects is nonlinear, but the determination of the current densities is linear and gives a good indication about the defect location and geometry.

This method has been applied to other types of defects, namely to small round holes. It has been able to detect holes with one millimeter in diameter.

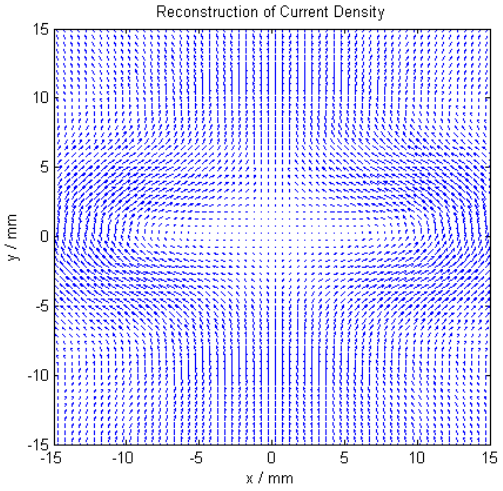


Figure 11. Reconstructed current around a crack.

## ACKNOWLEDGMENT

This work was developed under the Instituto de Telecomunicações projects KeMANDE and OMEGA and supported in part by the Portuguese Science and Technology Foundation (FCT) projects: PEst-OE/EEI/LA0008/2011, SFRH/BD/81856/2011 and SFRH/BD/81857/2011. This support is gratefully acknowledged.

## REFERENCES

[1] P.-Y. Joubert, Y. Le Bihan, “Multi sensor probe and defect classification in eddy current tubing inspection”, Sensors and Actuators A, vol.129, pp. 10-14, (2006).

[2] Ramos, H. G.; Ribeiro, A. L.; Pasadas, D.; Rocha, T.; “Modeling eddy current inspection of a metallic sample with round hole defects”, 18th Symposium IMEKO TC4 together with 9th International Congress on Electrical Metrology - IX Semetro, Natal, Brazil, September,2011.

[3] Dogaru, T.; Smith, S.T., “Giant magnetoresistance-based eddy-current sensor”, IEEE Transactions on Magnetics, Vol. 37, Issue 5, pp. 3831 – 3838, 2001.

[4] Non Volatile Electronics in www.nve.com.

[5] F. Corrêa Alegria, “Bias of amplitude estimation using three-parameter sine fitting in the presence of additive noise”, Measurement, Vol.42, N.5, pp.748-756, June 2009.

[6] M. A. Plonus, Applied Electromagnetics, McGraw-Hill, Ch. 6, pp.207-208, 1978.

[7] M. Bertero and P. Boccacci, Introduction to Inverse Problems in Imaging, Institute of Physics Publishing, Ch. 5, pp.98-136, 2002.